Materials Corrosion and Mitigation Strategies for APT, End of FY '97 Report:

I. Inconel 718 In-Beam Corrosion Rates from the '97 A6 Irradiation

R. Scott Lillard, Donald L. Pile, Darryl P. Butt

Materials Corrosion & Environmental Effects Lab
MST-6, Metallurgy Group
Los Alamos National Laboratory, Los Alamos NM 87545

January 1, 1998

submitted to:

Laurie Waters
APT - Technical Project Office
Los Alamos National Laboratory
Los Alamos, NM 87545

contributors:

Walter Sommer, APT-TPO
Stuart Maloy, APT-TPO
Gordon Willcutt, TSA-10
Richard Werbeck, LANSCE-7
Robert Brown, LANSCE-7
Eugene Zimmermann, MST-5/CON
Don Siebe, TSA-10
Keith Woloshun, ESA-EPE
Luke Daemen, LANSCE-LER
Greg Chandler, Westinghouse-SRS
Mike Barbe, MST-6
Jim Kachenko, MST-6

Summary of FY 1997 Accomplishments

The Corrosion sub-group of the APT Materials Irradiation Team successfully met all of its FY 1997 deliverables. The following is an abbreviated list of these accomplishments:

LANSCE-A6 Experiments:
1) design, procurement, and testing of in-beam corrosion probes with ceramic feed-through
2) procurement and testing of all other probes in the system including out-of-beam probes, hydrogen sensor, pH probes, conductivity probes
3) fabrication of water system and manifold for A6 experiments (LANSCE-7)
4) pre-irradiation testing of the A6 corrosion loop, associated equipment, and probes
5) measurement of in-beam corrosion rate for IN718 as a function of proton beam current
6) long term measurement of in-beam corrosion rate for IN718 at 1 mA
7) measurement of out-of-beam corrosion rates for IN718, SS304L, SS316L, Al6061, Al5052, W, and Ta in an irradiated water system
8) analysis and computer modeling of in-beam corrosion data
9) analysis and computer modeling of out-of-beam corrosion data
10) LA-UR # 97-0561, "Using Solution Resistivity as an Estimate of Tungsten Corrosion in Spallation Neutron Target Cooling Loops", by R.S. Lillard and D.P. Butt. (internal report)
11) LA-UR# 97-3854, "The Susceptibility of Materials in Spallation Neutron Source Target and Blanket Cooling Loops to Corrosion", by R.S. Lillard and D.P. Butt. (submitted to *Materials Characterization* for consideration in the APT Review Article)
12) LA-UR# 97-XXX, "Materials Corrosion and Mitigation Strategies for APT, End of FY '97 Report: I. Inconel 718 In-Beam Corrosion Rates from the '97 A6 Irradiation", by R.S. Lillard, D.L. Pile, D. P. Butt. (internal report)
13)LA-UR# 97-XXX, "Materials Corrosion and Mitigation Strategies for APT, End of FY '97 Report: II. Out-of-Beam Corrosion Rates and Water Analysis from the '97 A6 Irradiation", by R.S. Lillard, D.L. Pile, D. P. Butt. (internal report)

WNR Experiments:
Nov. 1996
1) design and fabrication of in-beam corrosion loop for use at WNR
2) in-beam corrosion rate measurements for tungsten as a function of beam current
3) analysis and computer modeling of in-beam tungsten data from WNR experiments
4) LA-UR# 97-3134, "Corrosion of Tungsten in an 800 MeV Proton Beam at the Weapons Neutron Research Facility", R.S. Lillard, D.P. Butt, (internal report).
June 1997
5) in-beam electrochemical experiments on W, Ta, SS304L, and Au as a function of beam current
6) in-beam Surface Enhanced Raman experiments of the passive oxide on W as a function of beam current
7) LA-UR# 97-5011, "Materials Corrosion and Mitigation Strategies for APT, Weapons Neutron Research Facility Experiments: The Effects of 800 MeV Proton Irradiation on the Corrosion of Tungsten, Tantalum, Stainless Steel, and Gold", R.S. Lillard, D.P. Butt, G. Kanner, L. Daemen. (internal report).

Laboratory Experiments
1) W corrosion rate measurements as a function of solution composition and pH
2) surface enhanced Raman measurements of the W passive oxide as a function of solution pH
3) LA-UR# XXX, The Nature of Oxides on Tungsten in Acidic and Alkaline Solutions and Their Role in the Dissolution Process", R.S. Lillard, G.S. Kanner, D.P. Butt. (to be submitted to *The Journal of the Electrochemical Society*).

Executive Summary

In-beam Corrosion Rates Electrochemical impedance spectroscopy (EIS) is a powerful technique that has been used by investigators for over 50 years to measure the corrosion rate of metals. Not only is EIS capable of measuring very low corrosion rates that would be immeasurable by weightloss or other "coupon" techniques, but also corrects for errors associated with solution resistance. For investigations were the solution resistance is high (such as DI water), uncompensated solution resistance may result in an underestimate of the actual corrosion rate.

During the FY '97 irradiation period, EIS was used to measure the polarization resistance (R_p) of Inconel 718 (IN718) as a function of beam current. Values of R_p as a function of beam current are show in Figure 1.es. Because the beam spot was small relative to the size of our IN718 corrosion probe (the beam width at 2σ was equal to 3 cm vs. the cylindrical probe dimensions of 1.3 cm in diam. x 15.9 cm in length), several methods for determining corrosion rate from R_p were derived. The first method used beam profile as a criteria for determining the area of highest damage. This damage profile may be anticipated if peak current were the controlling factor in the corrosion materials during proton irradiation. The beam spot intensity profile at LANSCE has been characterized and found to be a Gaussian distribution rotated about a central axis. The relationship between beam spot intensity and radial position is given by:

$$\phi_r = \phi_0 \exp\left\{-r^2 / 2\sigma^2\right\} \qquad (1.es)$$

where: φ_r is the flux in protons/cm^2 or μA/cm^2, r is the distance from the center of the beam in cm,

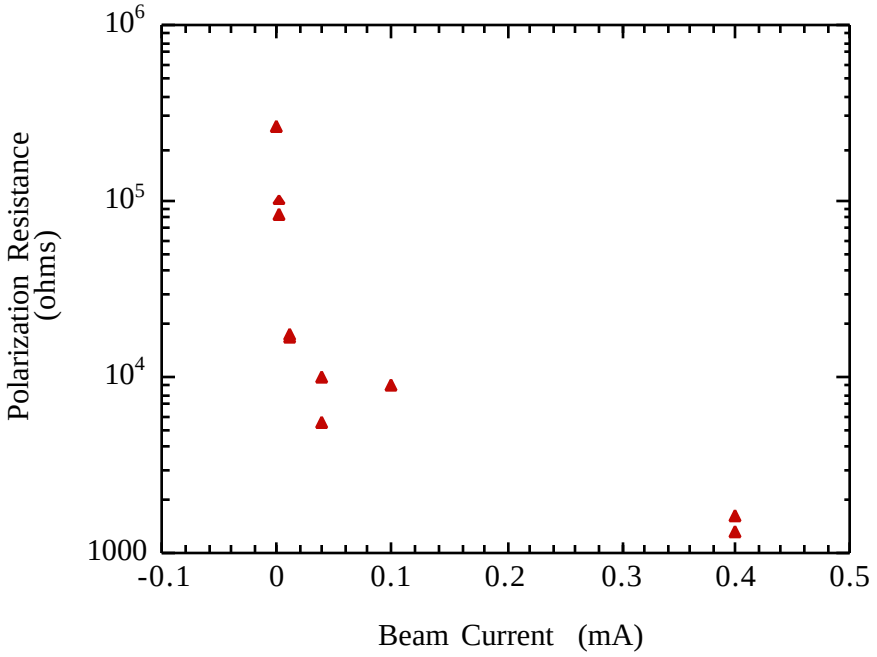

Figure 1.es IN718 polarization resistance as a function of beam current measured during irradiation at the LANSCE A6 Target Station.

σ is the standard deviation of a Gausian distribution and:

$$\phi_0 = I_t / 2\pi\sigma^2 \qquad \text{(2.es)}$$

For φ_r in μA/cm^2, I_t is equal to the beam current in μA. From this method, corrosion rate as a function of radial position from the center of the beam was generated for each beam current. Not surprisingly, the highest corrosion rates are at the center of the beam (r=0). These peak corrosion rates at r=0 are plotted in Figure 2.es as a function of beam current.

The second method for calculating corrosion rate from R_p assumed that the predominant area of corrosion was defined by a beam width at 2σ. Further, it assumed that the corrosion rate was uniform over this area. Specifically, R_p was multiplied by the area $\pi d \cdot 2\sigma$ where d was the diameter of the probe (1.3 cm). This damage profile may be anticipated if average proton flux were the controlling factor in the corrosion materials during proton irradiation. The third method used to calculate corrosion rate assumed that the distribution of corrosion was uniform across the entire surface. To calculate CR, R_p was multiplied by the total probe area (approximately 63.3 cm^2). This method is non-conservative and may be viewed only as a minimum corrosion rate.

As seen in Figure 2.es, the corrosion rate increases with increasing proton beam current for all three scenarios. Not surprisingly, the greatest corrosion rates are found when a Gaussian distribution is assumed. Physical evidence which suggests that a Gaussian distribution is an accurate depiction of corrosion rate as a function of position was found in the post-mortem analysis of a W rod in the front most bundle of the FY 96 17A insert. This insert was irradiated at 1 mA for approx. 2 months [Sommer, Maloy, Zaslawsky, Butt, Lillard, unpublished data]. Thickness

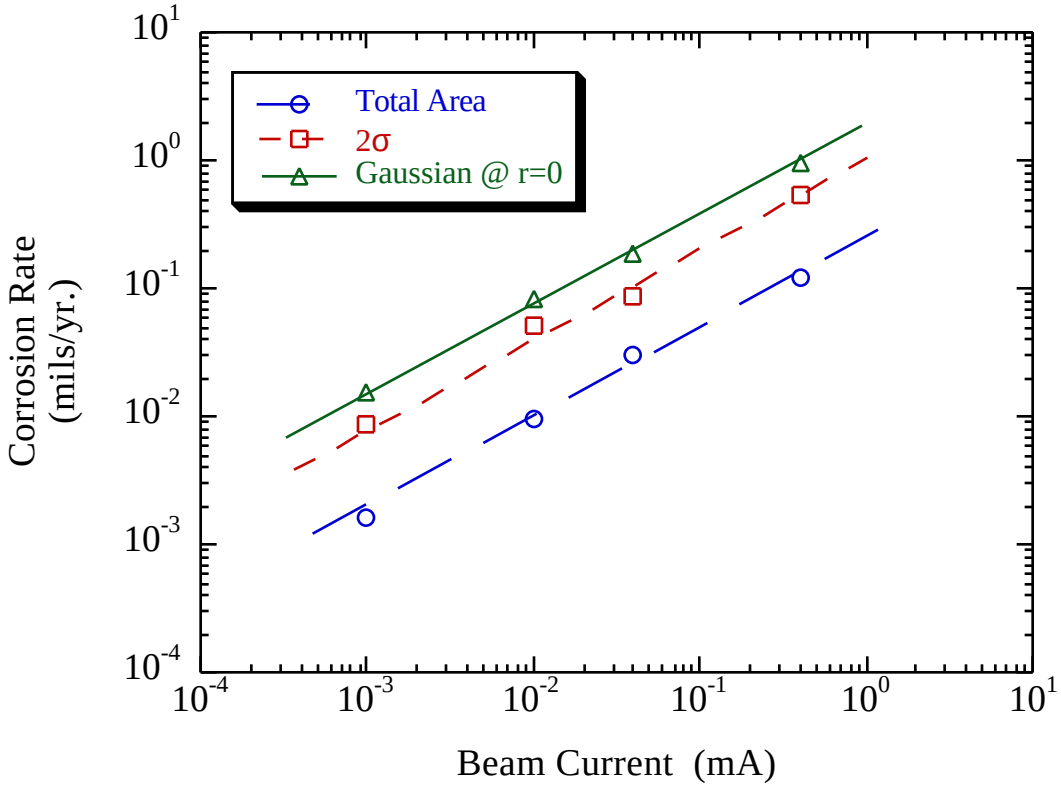

Figure 2.es Corrosion rate of in-beam IN718 probe as a function of beam current. Data has been calculated for several assumptions about the corroding area: 1) corrosion was uniform over the entire sample surface, 2) corrosion was limited to but uniform over an area defined by 2σ, and 3) corrosion was a function of proton flux as defined by Equation 1.es.

measurements of the rods found that the corrosion was greatest at the center of the rod (r=0) and decreased with increasing distance from r=0 in what appeared to be a Gaussian manner. *This finding, that the corrosion damage on the tungsten rods was distributed in a Gaussian manner from the center of the beam, is an indication that corrosion rate is dependent upon peak proton beam current and not average flux.*

The implication of Figure 2.es as it applies to the Accelerator Production of Tritium project is not yet clear. For example, the proposed APT beam will be rastered. This may have the same effect as the 100 Hz repetition rate of the beam at LANSCE, however this is not yet known. In addition, the APT proton beam will be operating at an energy of 1.7 GeV and a current of 1 mA. This energy and current is greatly different from those examined during the FY '97 LANSCE A6 Target Station. It is possible, however, to extrapolate the data from the FY '97 A6 irradiation to 1.0 mA. From Figure 2.es the relationship between beam current and corrosion rate was determined to be:

$$\log(CR) = \alpha + 0.68\log(BC) \qquad (3.es)$$

where BC is beam current in mA and α is a constant and is dependent upon the method used to calculate corrosion rate. From Equation 3.es, and the Gaussian assumption (i.e. corrosion rate is a function of distance from the center of the proton beam; $\alpha = 0.25$), the corrosion rate of IN718 at the center of a 1.0 mA proton beam would be approximately 0.002" per year. However, this rate is based on the LANSCE A6 beam profile (Equation 1.es) and, consequently, the actual corrosion rate for an in-beam IN718 sample at APT may vary. Currently, we are exploring a method for relating the in-beam corrosion rates measured at the LANSCE A6 Target Station to the APT beam. It may also be noted that the EIS probes and in-beam weightloss foils will be visually examined and weighed during hot-cell operations.

System calibration The equipment used to make the IN718 in-beam corrosion rate measurements was calibrated by the manufacturer prior to shipment in 1996. In preparation for the FY '98 irradiation, this equipment was sent back to the manufacturer for calibration in the fall of 1997. As of December 1, 1997 these systems have been calibrated to NIST traceable registry numbers: 10071, 10072, and 10073. Current records of system calibration are available upon request.

Table of Contents

List of Tables

List of Figures

Introduction

This report summarizes our results from the 1997 irradiation of the corrosion insert at the LANSCE A6 Target Station. It addresses the corrosion measurements made on the in-beam Inconel 718 probe only. Results from the out-of-beam corrosion probes discussing the effects of radiolyzed water on the corrosion rates of Al 6061, Al 5052, tungsten, Inconel 718, tantalum, stainless steels 304 and 316, and Hastelloy C276 will be presented in separate report: "Materials Corrosion and Mitigation Strategies for APT, End of FY '97 Report: II. Out-of-Beam Corrosion Rates from the '97 A6 Irradiation Period." This second report has a later release date.

To simulate the environment that materials may be exposed to in a spallation neutron target / blanket cooling loops, samples were irradiated by the proton beam at the A6 Target Station of the Los Alamos Neutron Scattering Center (LANSCE). To accomplish this, a cooling water loop capable of exposing corrosion samples to an 800 MeV proton beam at currents upwards of 1 mA was constructed. This loop allowed control and evaluation of hydrogen water chemistry, water conductivity, and solution pH. To measure real-time corrosion rate in the beam, it was necessary to electrically isolate the probes from the water system with a material that was capable of withstanding the this environment. To accomplish this, specially designed ceramic sealed probes were fabricated. These probes allowed materials to be placed directly in the proton beam. The real-time corrosion rate of these materials was measured with electrochemical impedance spectroscopy (EIS).

Experimental

Design and Fabrication of the Corrosion Loop The in-beam corrosion experiments in this investigation were carried out at the LANSCE A6 Target Station located in Experimental Area A just in front of the linac beam stop. While the A6 Target Station provides the investigator with a 1 mA, 800 MeV proton beam, it was necessary to design and fabricate a cooling water loop that would allow us access to it. A diagram representing the corrosion water system at the A6 Target Station is presented in Figure 1. This is a closed-loop system filled with de-ionized water. The

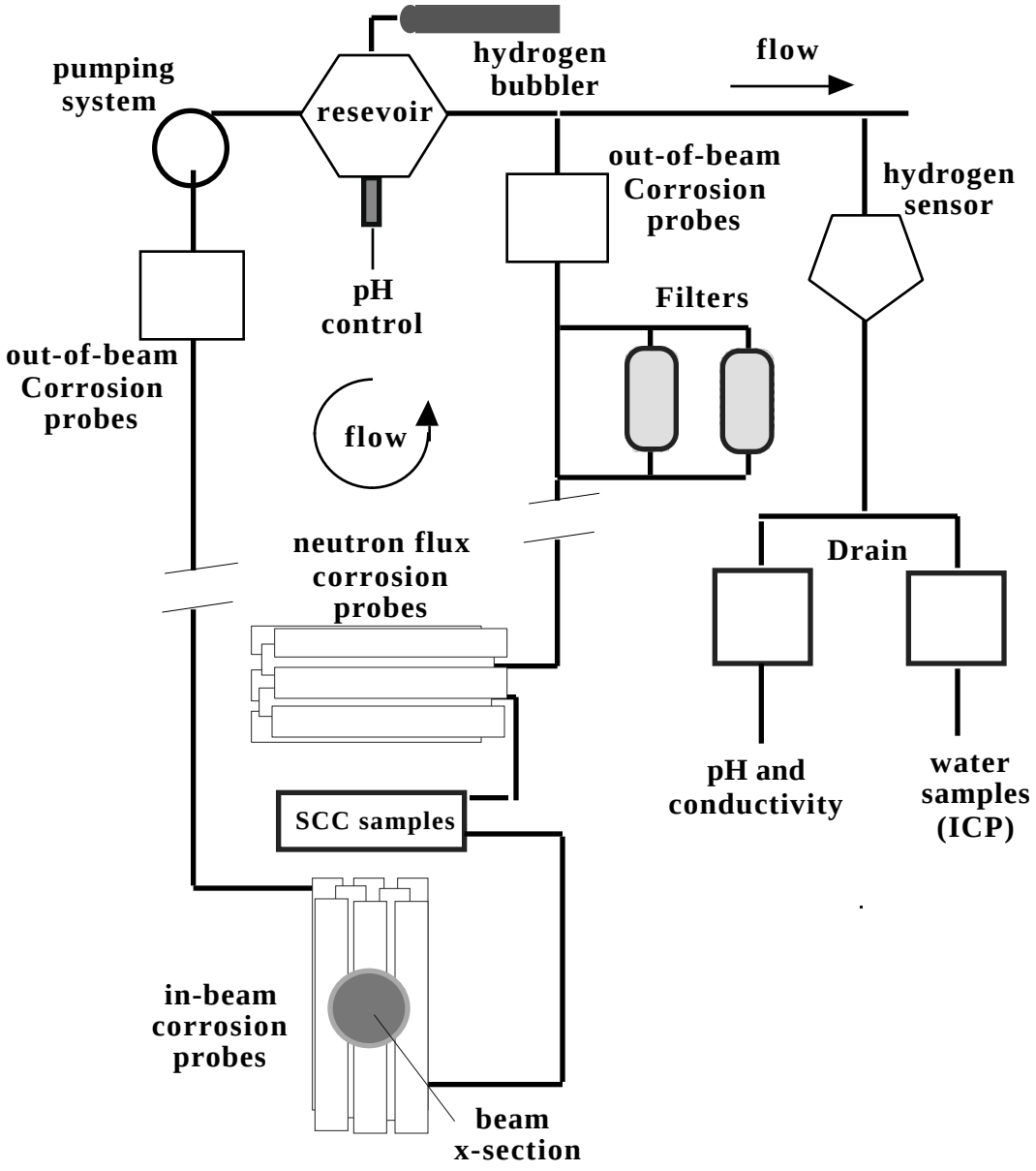

Figure 1 A diagram representing the corrosion diagnostics to be used on the cooling water loop at the LANSCE A6 target station. The proton beam is perpendicular to the diagram and is represented by the oval over top the in-beam corrosion probes

pump nominally operates at 150 psi and a flow rate of 10-20 gal/min.

The in-beam corrosion probes are represented by the rectangular tubes at the bottom of Figure 1. The beam path is perpendicular to the page. These probes were placed directly in the proton beam to evaluate the effects of the proton beam interactions as well as short lived and long lived radiolysis products on corrosion rate.

In-Beam Corrosion Probes One of the major goals of this program was the design and fabrication of corrosion probes to be used in-beam at the LANSCE A6 Target Station. To measure corrosion rate, it was necessary to electrically isolate the corrosion sample from the cooling water loop. Conventionally, this can be accomplished with metal-to-glass seals. However, irradiation of the glass may cause it to become conductive, rendering the seal useless. Therefore, an alternate sealing method was chosen. As shown in Figure 2, the corrosion samples were hollow rods (one end closed, one end open) measuring 0.5" in diameter and 6.25" in length. To electrically isolate the test specimen from the water system, the open end of each corrosion sample was joined to a dumb-bell shaped ceramic by means of a compression seal. Because the corrosion samples had high thermal expansion coefficients, the ceramic chosen for this application was alumina. The other end of the ceramic was joined to a stainless steel 304L (SS304L) flange by means of another compression seal. This flange provided a means of welding the probe assembly into the water system. The temperatures required to form the compression seal (approximately 1000^{o} C) ruled out the possibility of examining the corrosion rate of aluminum alloys in-beam. It may also be noted that because the materials used to make the in-beam probes (both samples and flange material) had low carbon concentrations and the amount of time at 1000^{o} C was minimal, sensitization was not an issue.

A diagram of the water manifold that housed the in-beam corrosion probes is presented in Figure 3. This manifold consisted of 7 tubes arranged in a close packed array with tube #1 being in the front-most position. Each tube contained either an in-beam corrosion probe with ceramic (noted as EIS) or a weightloss foil (2" x 5/16" x 1/16") made from W, SS 304L, or Ta (noted as **wl** in Fig. 3). This manifold was welded to the bottom of an 11' supporting insert which not only supported the manifold but also provided the necessary conduits for electrical and water connections. A diagram depicting the corrosion insert and its relative position at the target station is presented in Figure 4 as insert 17B.

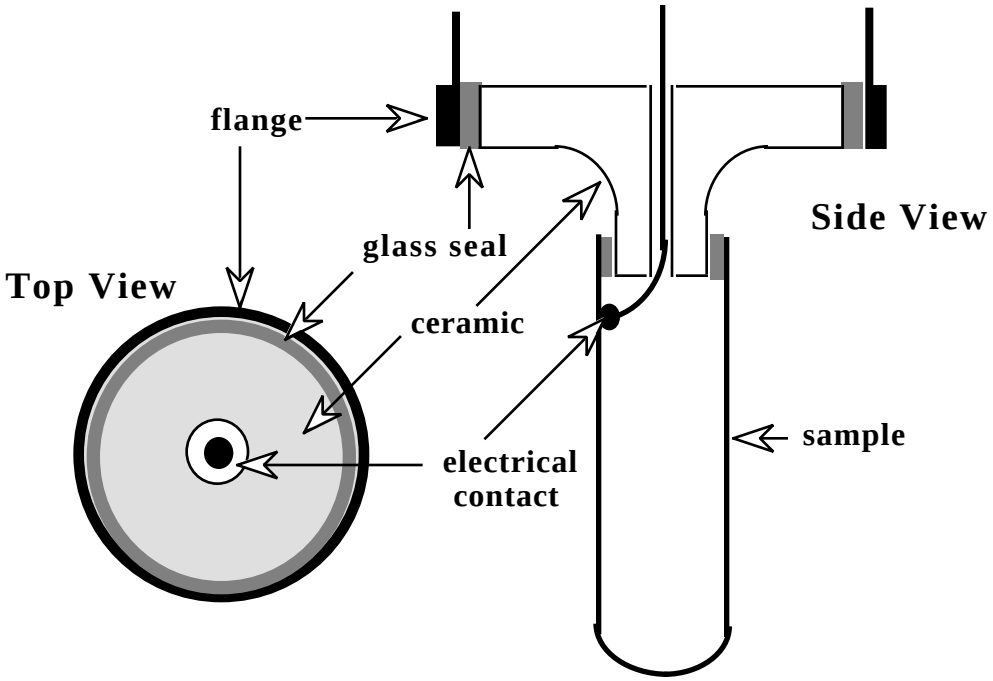

Figure 2 In beam corrosion probe showing ceramic feedthrough and compression seals (not drawn to scale.

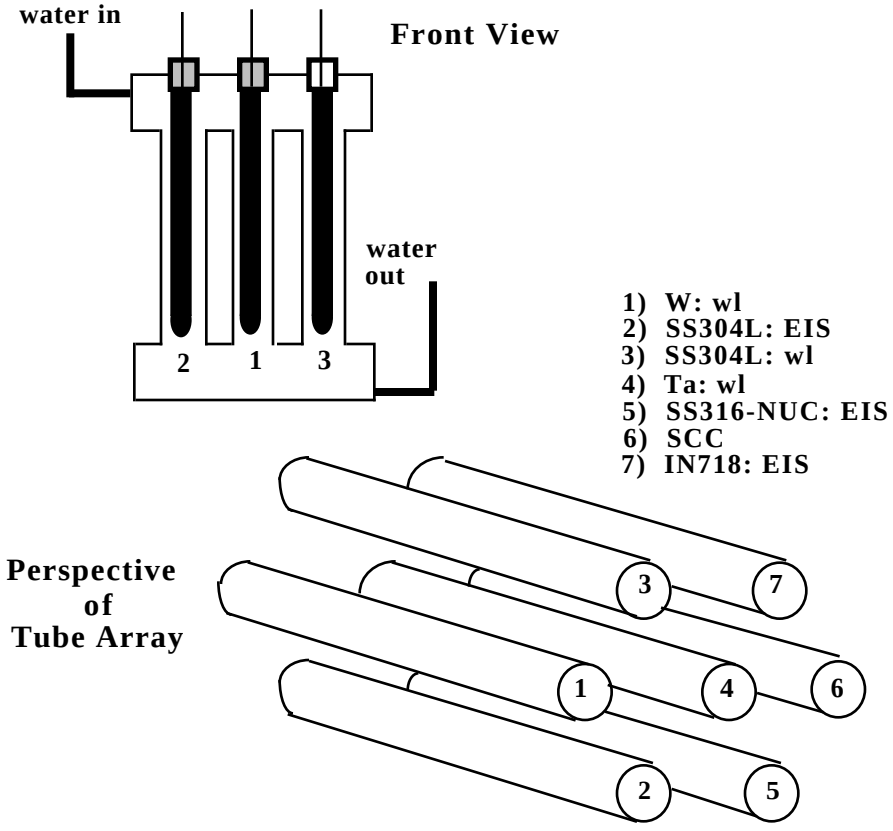

Figure 3 A diagram representing the placement of the in-beam corrosion probes in the manifold section of the cooling water loop.

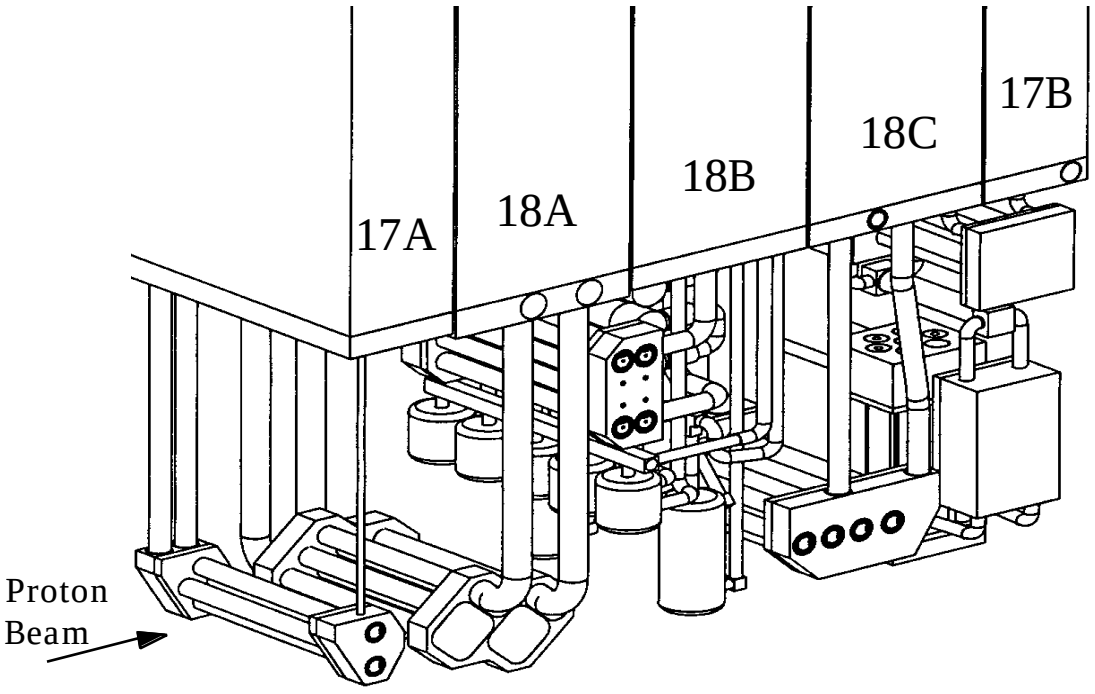

Figure 4 Diagram depicting inserts at the LANSCE A6 Target Station. The insert containing the corrosion samples is labeled 17B. The approximate length of the insert (including the manifold) is 11'. The associated closed loop water system is not shown.

Sample Preparation and Water Quality Prior to placing the in-beam corrosion probes and weightloss samples in the water system they were ground to 600 grit using SiC paper. After grinding, the samples were degreased in an ultrasonic bath of acetone. Degreasing was followed by successive ultrasonications in ethanol and de-ionized water. The interior of the water system which includes all piping, tanks, and pumps was steam cleaned and rinsed with a mixture of water and ethanol after assembly. The water system was then filled with DI water (approximately 60 gallons), operated for several hours then flushed. This was repeated three times before the final system fill with DI water. Nominally, the water in the system had a resistivity of $8x10^4$ ohm cm. Ion coupled plasma analysis of a water sample taken from the system after running for several days, prior to irradiation, found: 0.01μg/ml W, 0.03 μg/ml Mg, 0.01 μg/ml Fe, 0.04 μg/ml Zn, 0.02 μg/ml Cu, and 2.6 μg/ml Ca. Nominally, the system operated at a water temperature of approximately 30^o C +/- 2, 150 psi and a flow rate of 10-20 gpm. It may also be noted that the

system was operated with a dissolved hydrogen concentration of approximately 0.40 ppm. This was accomplished by continuously bubbling 6% H_2 - 94% Ar gas into the system's receiver tank.

Proton Beam Characteristics The proton beam at LANSCE had a characteristic macropulse repetition rate of 100 Hz and a gate length of 625 microseconds (Figure 5). Beam currents were controlled by varying the spacing between each micropulse (and therefore the number of micropulses) in the gate. The initial experiments were conducted at proton beam currents of 0.001, 0.010, 0.04, 0.10, and 0.40 mA. These data were taken with all other inserts (17A - 18C in Figure 4) pulled out of the proton beam such that the first material that the proton beam struck after leaving high vacuum was tube #1 of the corrosion manifold (17B). Thermocouples attached to the front of the manifold verified the position, size and shape of the proton beam (Figure 6).

After approximately 10 days of experiments with only the corrosion insert in place, the 17A, 18A, 18B, and 18C inserts were placed back in position and the beam current was increased to 1.0 mA. The effect of these inserts in front of the corrosion insert was to spread the proton beam from its compact Gaussian distribution where $2\sigma = 3$ cm, to a more uniform fluence over a slightly larger area.

Electrochemical Measurements As discussed above, EIS was used to measure the corrosion rate of the in-beam probes as a function of beam current and irradiation time. These measurements were conducted with a 30 mV sinusoidal voltage perturbation over the frequency range of 0.005 - 1 kHz. No applied dc potential was employed; that is, all measurements were conducted at the Open Circuit Potential (OCP). To eliminate the effects of ground loops, floating ground EIS systems were used. As a reference electrode was not capable of withstanding the proton / neutron flux at the manifold, a 2 electrode EIS measurement was employed. In this measurement the water system (ground) acted as both reference and counter electrodes. This was made possible by the large area of the water system. Although the specific resistivity of the SS304 system was large ($>10^6$ ohm cm^2) because its surface area was also large, the measured resistance was small (less that 10 ohms). The validity of this method was confirmed by EIS measurements

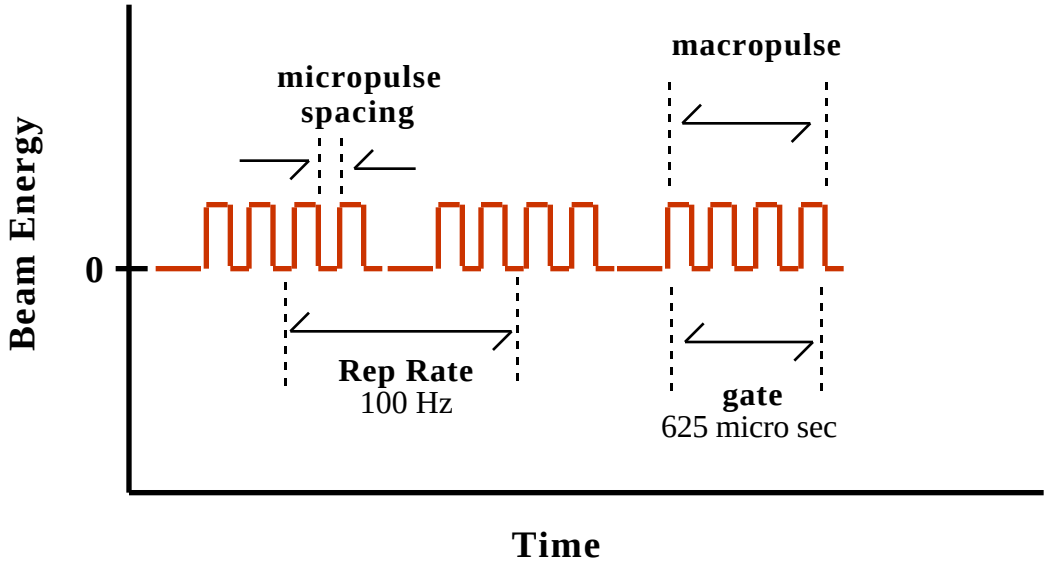

Figure 5 Diagram depicting the characteristics of the proton beam at the LANSCE A6 Target Station

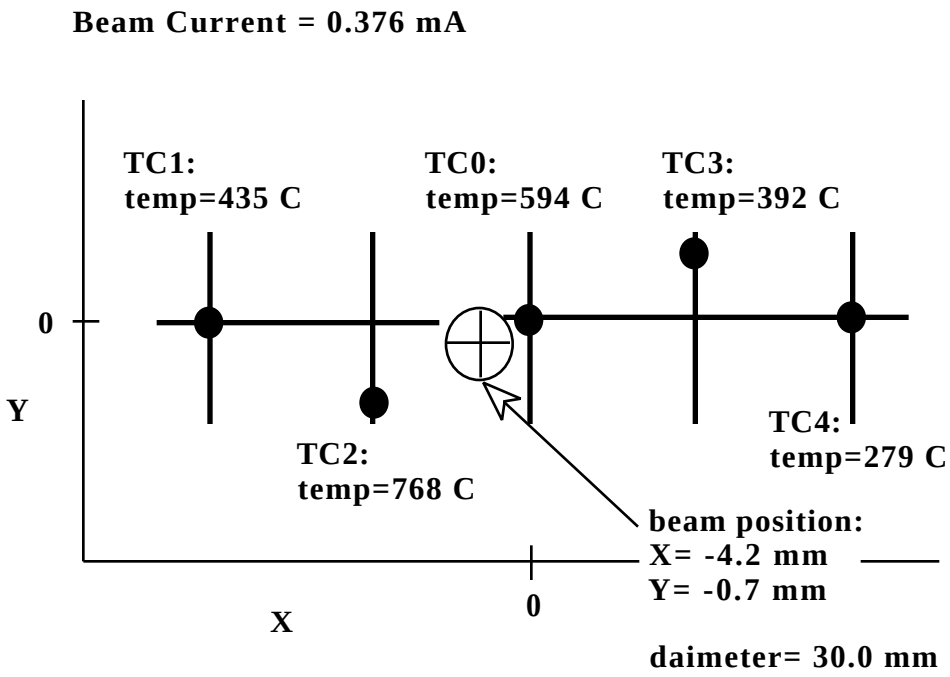

Figure 6 Diagram representing the thermocouple grind welded to the front of the 17A insert. An algorithm based on thermocouple temperature was used to steer the beam as close as possible to the center of Tube 1 (0,0) and calculated its approximate diameter. Thermocouple temperatures and calculation of beam size and position are shown for a beam current of 0.4 mA and no other inserts in front of 17A.

on the three electrode out-of-beam probes. In these experiments, the results from three electrode EIS experiments were compared to 2-electrode measurements using the same working electrode and the water system as the reference and counter electrodes. This is the same configuration as used in the in-beam measurements. Identical results were obtained from the 2-electrode and 3-electrode configurations. Moreover, the area normalized polarization resistance of the in-beam IN718 probe was identical to the area normalized polarization resistance from the out-of-beam IN718 sample with the beam off.

Results and Discussions

Pre-Irradiation Measurements Prior to placing the insert in the proton beam, the polarization resistance of the in-beam corrosion probes was compared to the polarization resistance of the out-of-beam corrosion probes. Because multiple out-of-beam samples for each material existed, probes were used as standards for comparison. Unfortunately, only the data from the IN718 in-beam probe could be verified against the out-of-beam samples. Therefore, only data from the IN718 probe was measured and reported on.

In-beam EIS Measurements Typical EIS data from the IN718 in-beam corrosion probe as a function of beam current are presented in Figure 7 in the form of Bode magnitude and phase plots. It may be noted that the magnitude of the impedance (|Z|) is presented in ohms and not the traditional $\text{ohm} \cdot \text{cm}^2$. A complete discussion of area, relative to the proton beam spot size is addressed in the following section. As seen in Figure 7a, the low frequency limit of the IN718 data decreased with increasing proton beam current. As only one time constant was observed, the EIS data were modeled by the simplified Randles equivalent circuit (EC) shown in Figure 8 where: R_p is the polarization resistance, C_{dl} is the capacitance associated with the double layer, and R_{sol} is the geometric solution resistance between the sample and the water system. A complex non-linear least squares (CNLS) fit of the in-beam data at a proton current of 0.400 mA to this EC is presented in Figure 9. As seen in this figure, good agreement between the model and the data

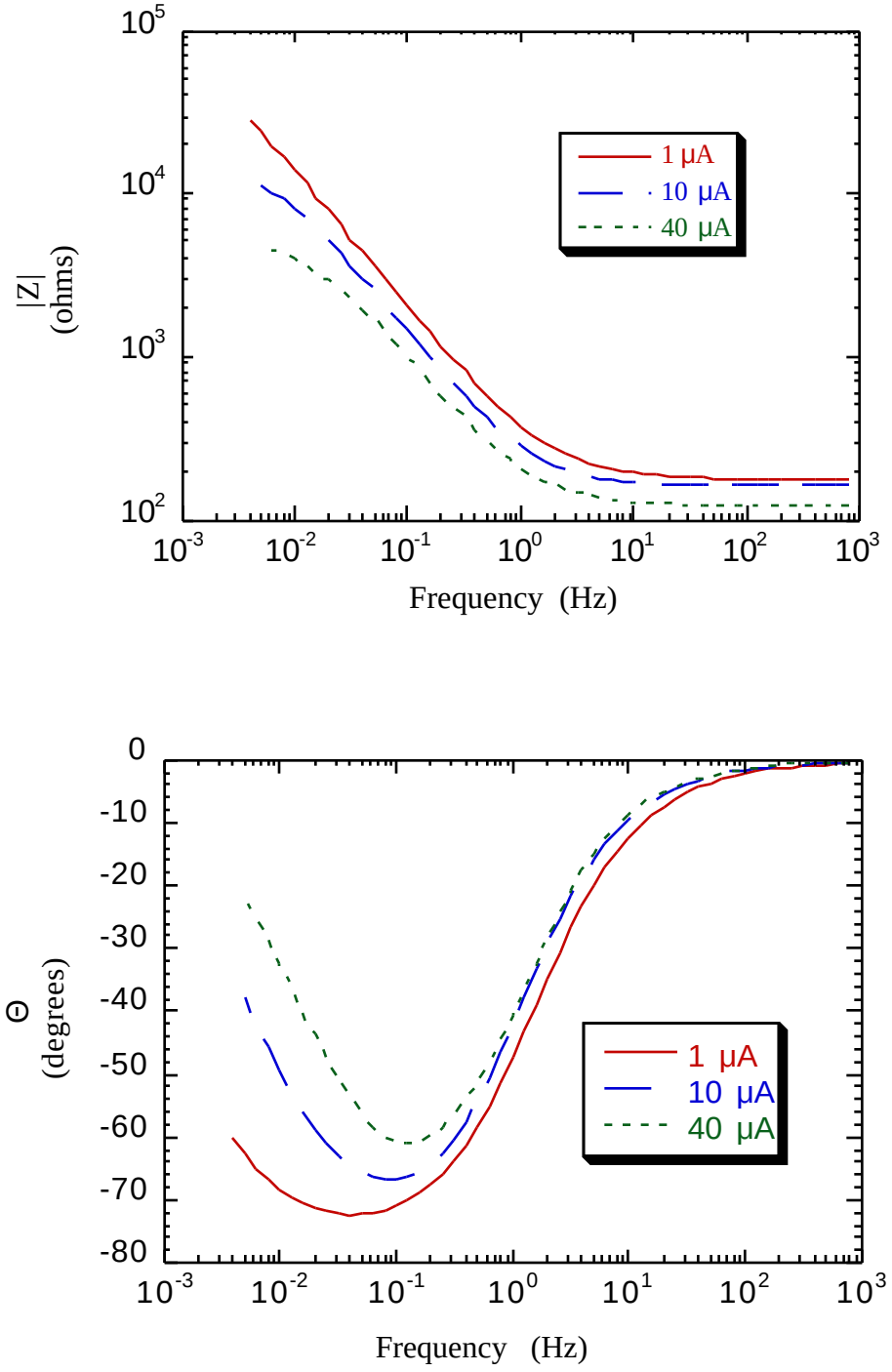

Figure 7 Typical **a)-top** Bode Magnitude and **b)-bottom** Bode phase plots from the in-beam IN718 probe as a function of beam current

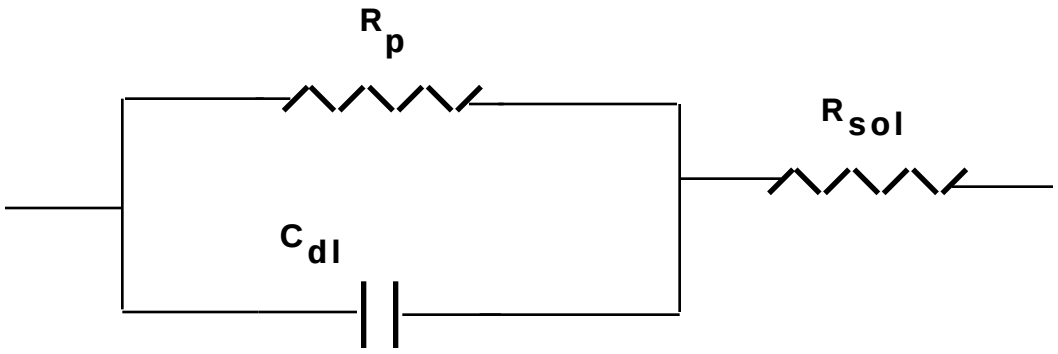

Figure 8 Simplified Randles circuit used to model EIS data taken at early irradiation times

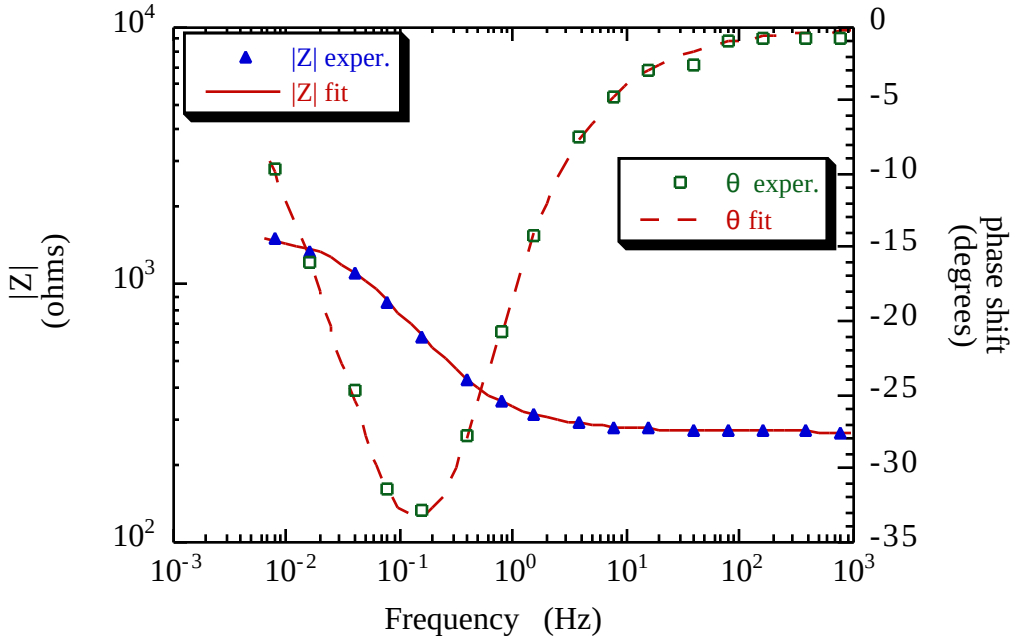

Figure 9 Experimental EIS data taken at 0.40 mA with no other inserts in front of 17B and the CNLS fit of the EC in Figure 8 to the data. Note, only 20% of the experimental data are shown for clarity.

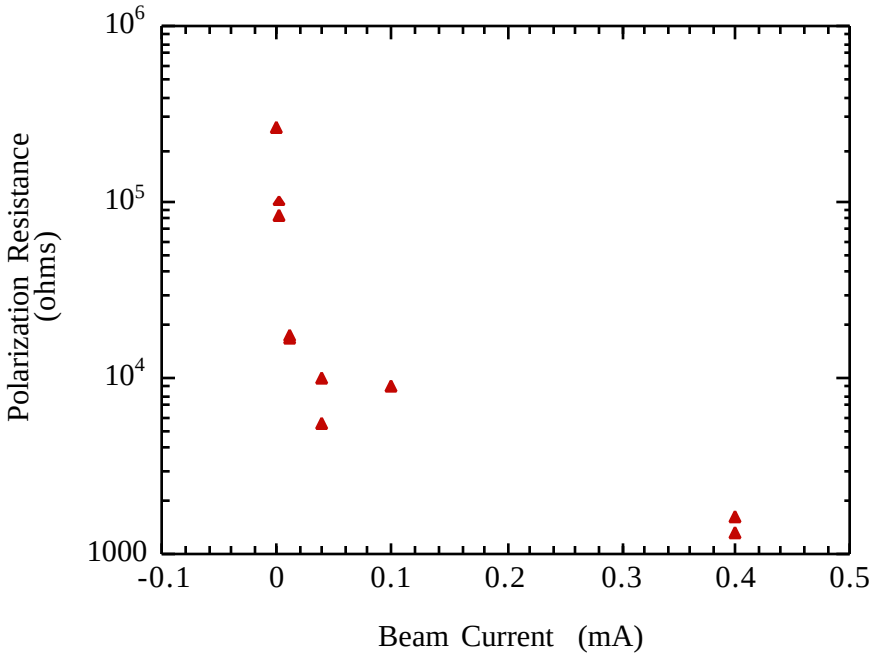

Figure 10 Polarization resistance from the in-beam IN718 probe (measured by EIS) as a function of beam current.

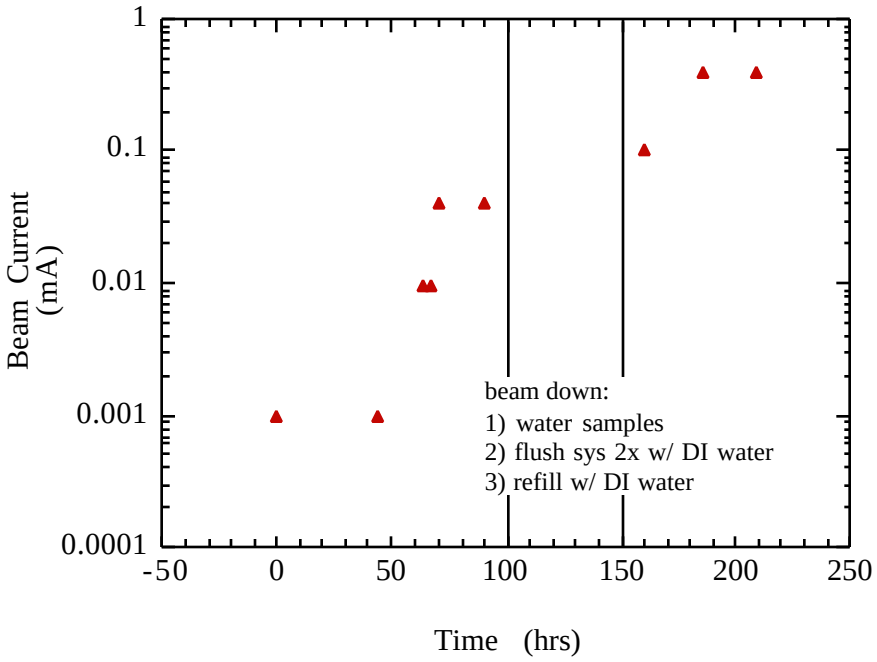

Figure 11 Beam currents from Figure 10 as a function of time.

exists. The polarization resistances obtained from CNLS fitting as a function of proton beam current are presented in Figure 10. The corresponding beam current as a function of time is presented in Figure 11. As seen in Figure 10, an exponential decrease in R_p with increasing beam current was observed.

In-beam Corrosion Rates Because the beam spot was small relative to the size of our IN718 corrosion probe (the beam width at 2σ was equal to 3 cm vs. probe dimension of 1.3 cm in diam. x 15.9 cm in length), several methods for determining corrosion rate from R_p were derived. The first method used beam profile as a criterion for determining the area of highest damage. The beam spot intensity profile at LANSCE has been characterized and found to have a Gaussian distribution rotated about a central axis. The relationship between beam spot intensity and radial position is given by:

$$\phi_r = \phi_0 \exp\left\{-r^2 / 2\sigma^2\right\} \qquad (1)$$

where: ϕ_r is the flux in protons/cm^2 or μA/cm^2, r is the distance from the center of the beam in cm, σ is the standard deviation of a Gausian distribution. For ϕ_r in μA/cm^2:

$$\phi_0 = I_t / 2\pi\sigma^2 \qquad (2)$$

where I_t is equal to the beam current in μA. For our study 2σ was equal to approximately 3 cm (σ =1.5 cm) and I_t was varied from 1-400 μA. Assuming that the corrosion occurs preferentially in the beam and is a function of proton flux, a relationship between polarization resistance (in ohm$\cdot$ cm^2) and beam intensity profile can then be established from equation 1:

$$R_p^G = b \Big/ \left(\phi_0 \exp\left\{-r^2 / 2\sigma^2\right\}\right) \qquad (3)$$

where R^G_p is the Gaussian distribution of the polarization resistance in ohm$\cdot$ cm^2 and **b** is a constant in units of ohm$\cdot$ cm$^2\cdot\mu$ A that was determined by fixing the average R_p ($\overline{R}_p$) to an area bound by 2σ of the proton beam:

$$\bar{R}_p = R_p \quad (2\sigma \quad \pi d) \tag{4}$$

$$b = \bar{R}_p \left(\phi_0 \exp\left\{ -\sigma^2 / 2\sigma^2 \right\} \right) \tag{5}$$

where d is the diameter of the probe (equal to 1.27 cm) and R_p is in units of ohms not ohm$\cdot$ cm^2.

From R^G_p, the density of IN718 (ρ=8.19g/cm^3), the equivalent weight of IN718 (EW=25.66 grams/equivalent), and assuming Tafel slopes of 0.12 V/decade the corrosion rate in mils/yr. was determined as a function of position (r) from the center of the beam:

$$CR^G(r) = \frac{129\left(2.6/R_p^G\right)(EW)}{\rho} \tag{6}$$

The Gaussian distribution of the corrosion rate (CR^G(r)) for the in-beam IN718 probe for beam currents of 0.04 and 0.4 mA is presented in Figure 12. As may be anticipated for this distribution, the highest corrosion rates are found at the center of the probe (r=0). For a beam current of 0.40 mA the theoretical value for the FWHM is 3.26 cm. As shown in Figure 12, the FWHM for the calculated corrosion profile at a beam current of 0.40 mA is 3.5 cm. Physical evidence which suggests that this distribution is an accurate depiction of the corrosion rate as a function of position is presented in Figure 13. These data were taken from a W rod in the front most bundle of the 17A insert after the Fall 1996 irradiation period [Sommer, Maloy, Zaslawsky, Butt, Lillard, unpublished data]. The insert was irradiated at a beam current of 1.0 mA for approximately 2 months. As shown in this plot, there appears to be two modes of corrosion damage, mass transport effects (water velocity) and proton damage. The mass transport effects are characterized by a thinner rod diameter on the inlet side as compared to thickness differences on the outlet side. There is also a possibility that this is an erosion effect, however, particle concentration was controlled by filters (200 and 2 x10^{-6} m) and regular flush/refill of the water system. The beam effects are characterized by the Gaussian shape of the rod thickness near its center. Although the corrosion damage near the center of the probe appears to be mixed mode, it is interesting to note

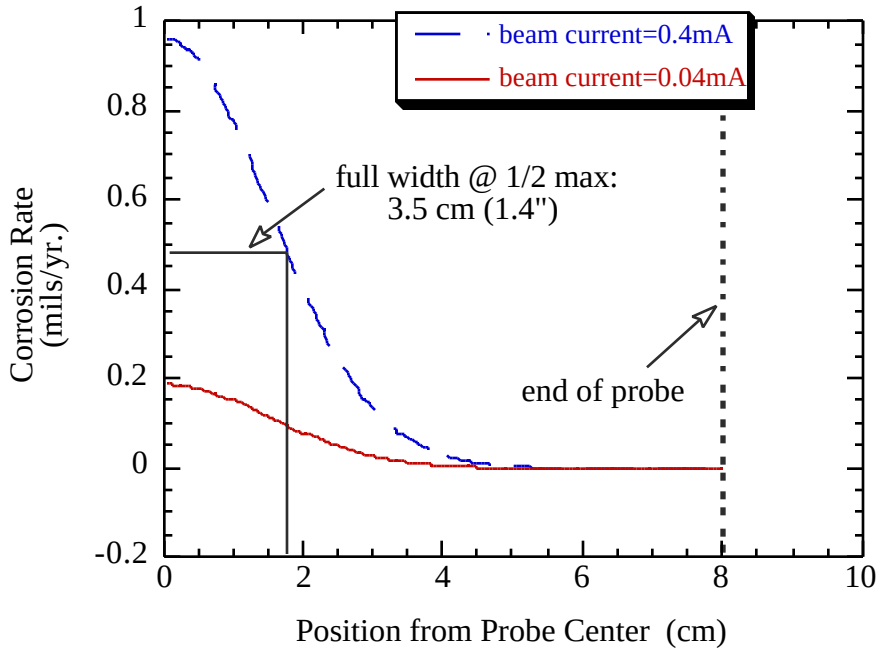

Figure 12 Corrosion rate as a function of radial distance from the beam (probe) center as calculated from Equation 6.

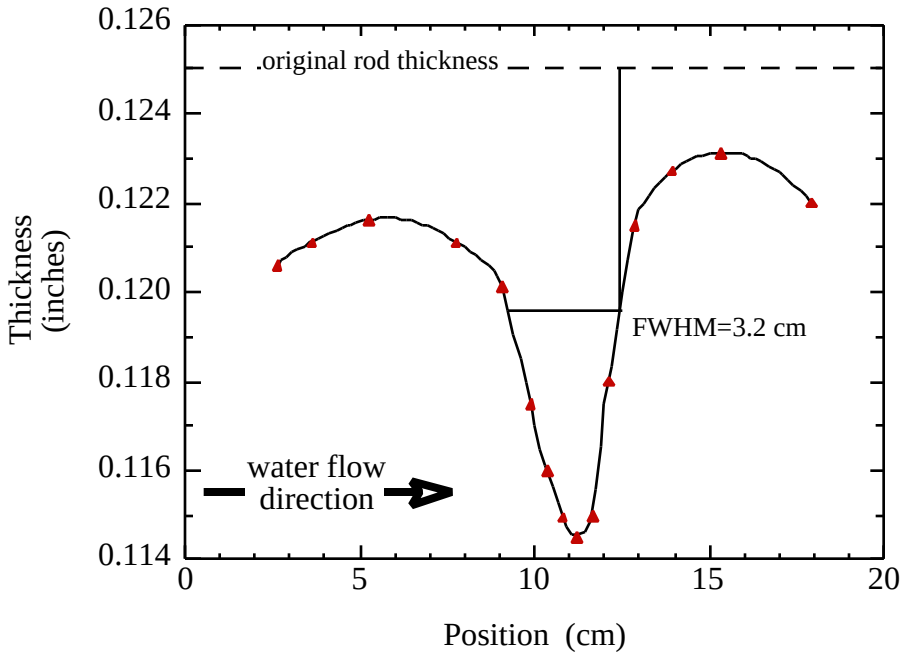

Figure 13 Thickness changes in a 0.125" diameter tungsten rod after proton irradiation at 1.0 mA for 2 months (Maloy, Sommer, Zaslawsky, Butt, Lillard, unpublished data.

that the full width at half of the maximum (FWHM) is approximately 3.2 cm. The theoretical FWHM for a beam current of 1.0 mA is 3.46 cm. Moreover, the data in Figure 13 is an indication that corrosion rate is dependent upon peak beam current and not average flux.

The peak corrosion rates (i.e., at r=0) are presented in Figure 14 as a function of beam current. The data points in this plot are the average of three measurements. In addition to the corrosion rates at r=0 from the Gaussian distributions, Figure 14 also plots corrosion rate as a function of proton beam current for two other scenarios. The first scenario assumed that the predominant contributor to the corrosion current comes from an area defined by 2σ. Further, it assumed that the corrosion rate was uniform over this area. Specifically, R_p was multiplied by the area $\pi d \times 2\sigma$ where d was the diameter of the probe and equal to 1.3 cm. The second scenario assumed that the distribution of corrosion was uniform across the entire surface. To calculate CR, the measured polarization resistance (R_p) was multiplied by the total probe area (approximately 63.3 cm^2). This rate is non-conservative and should be used to assess the minimum corrosion rate only. As seen in Figure 14, the change in corrosion rate as a function of beam current was similar for all three assumptions and can be defined by the relationship:

$$\log(CR) = \alpha + 0.68\log(BC) \qquad (7)$$

where BC is beam current in mA and α is a constant and is dependent of the method used to calculate corrosion rate. The values for α are: 0.25, 0.043, and -0.68 for the Gaussian, 2σ, and total probe area assumptions, respectively as discussed above.

It should be noted that the peak corrosion rates calculated from the Gaussian distribution above are valid for the LANSCE A6 beam profile only.

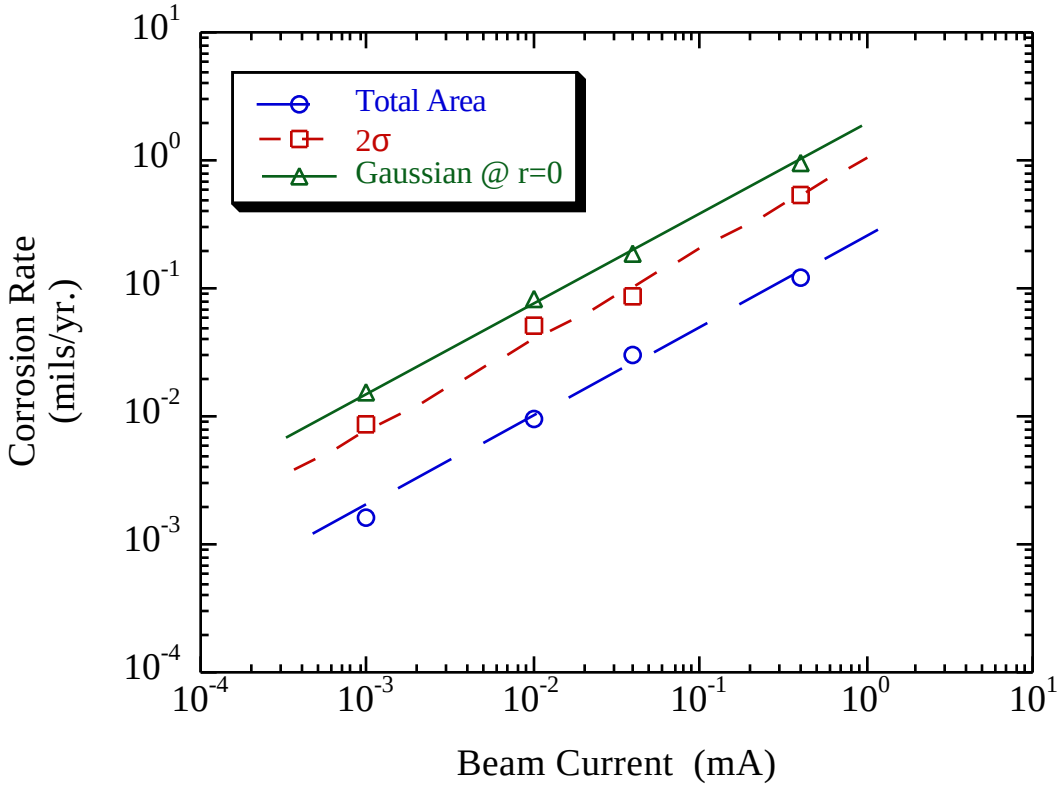

Figure 14 Corrosion rate of in-beam IN718 probe as a function of beam current. Data has been calculated for several assumptions about the corroding area: 1) corrosion was uniform over the entire sample surface, 2) corrosion was limited to, but uniform over an area defined by 2σ, and 3) corrosion was a function of proton flux as defined by Equation 1.

Long Term Irradiation Measurements In addition to corrosion measurements at low current where only the corrosion insert was exposed to the proton beam, measurements were also made at a proton beam current of 1.0 mA with the four other inserts (17A and 18A-C) in front of 17B. As discussed above, having these inserts in front of 17B causes the beam to be widely spread by the time it reaches the corrosion insert. During this period, EIS data from the in-beam IN718 probe was gathered every 7-10 days. After approximately 1400 hrs. (with all inserts in place and the beam operating at 1.0 mA), the impedance data began to show evidence of a diffusion component. The effect of this diffusional impedance can be seen in Bode magnitude data presented in Figure 15. In the frequency range of 1 to 0.04, the slope is equal to -1, which is the

characteristic response of a capacitor. Below approximately 0.04 Hz the Bode magnitude data has a slope of -1/2 which is the characteristic response of a diffusional (Warburg) impedance. Therefore, the data collected after 60 days of immersion was model by a slightly different equivalent circuit than that used for data gathered at earlier immersion times. This EC is presented in Figure 16 where **W** represents the traditional Warburg type impedance and all other elements are as before (Figure 8). The CNLS fit of the model to the experimental data is also presented in Figure 15. As seen in this figure, excellent agreement between the model and the experimental data exists.

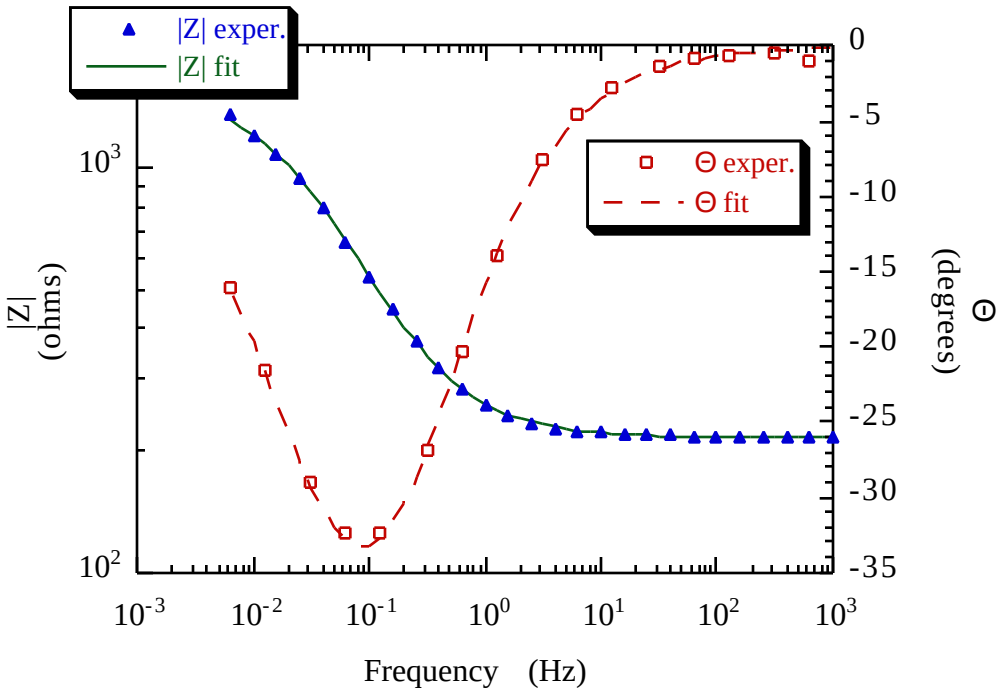

Figure 15 Typical EIS data from the in-beam IN718 probe taken after 1440 hrs of immersion. The Warburg impedance is noted by the change in slope at 0.04 Hz from -1 at higher frequencies to -1/2 at lower frequencies. Note, only 20% of the experimental data is shown for clarity.

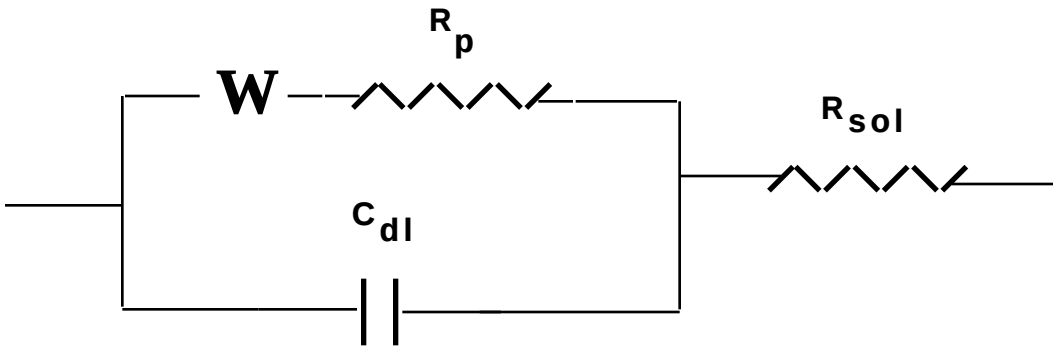

Figure 16 Equivalent circuit used to model the in-beam EIS data at longer irradiation times.

The polarization resistance of the IN718 probe as a function of irradiation time is presented in Figure 17. The data are presented in units of ohms and not ohm$\cdot$ cm^2 for the reasons addressed above. Although some scatter in the long-term data was observed, R_p remains fairly constant as a function of time with all inserts in place and the beam operating at 1.0 mA. The observation that R_p did not decrease upon increasing the beam current to 1.0 mA (at 300 hrs) is likely due to spreading of the beam after striking the four front inserts. The data taken at 2400 hr with the beam on and the 17B insert raised approximately 1-2 feet above the beam also shows the effect of the 4 front inserts. With the beam on and the insert in place, R_p was 2.0 x10^3 ohms. The effect of raising the insert two feet above the beam is seen in the data collected 24 hrs later where R_p was 6.8 x10^3 ohms, a value that is only slightly below the scatter. The observation that R_p did not return to its pre-irradiation value is likely due to the spreading of the proton beam and the high neutron flux in this area that arises from the beam striking high Z-number materials (such as tungsten) in the front inserts.

It may also be noted that by the end of the irradiation period beam trips (the on/off cycling of the beam) became very frequent (Figure 18). The only data presented in this study were collected during periods that contained no beam trips.

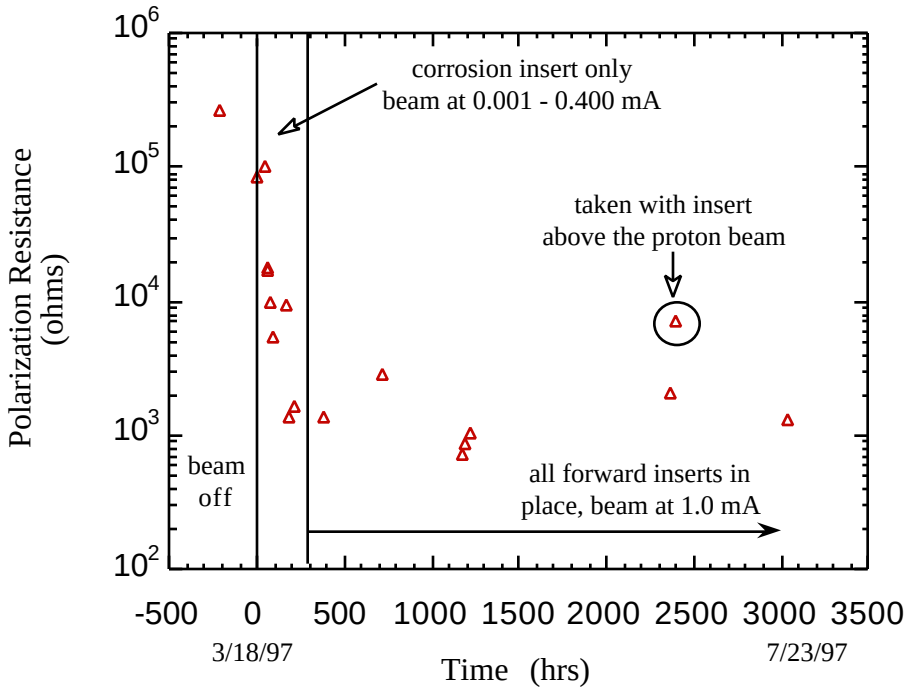

Figure 17 Polarization resistance of the in-beam IN718 probe as a function of irradiation time.

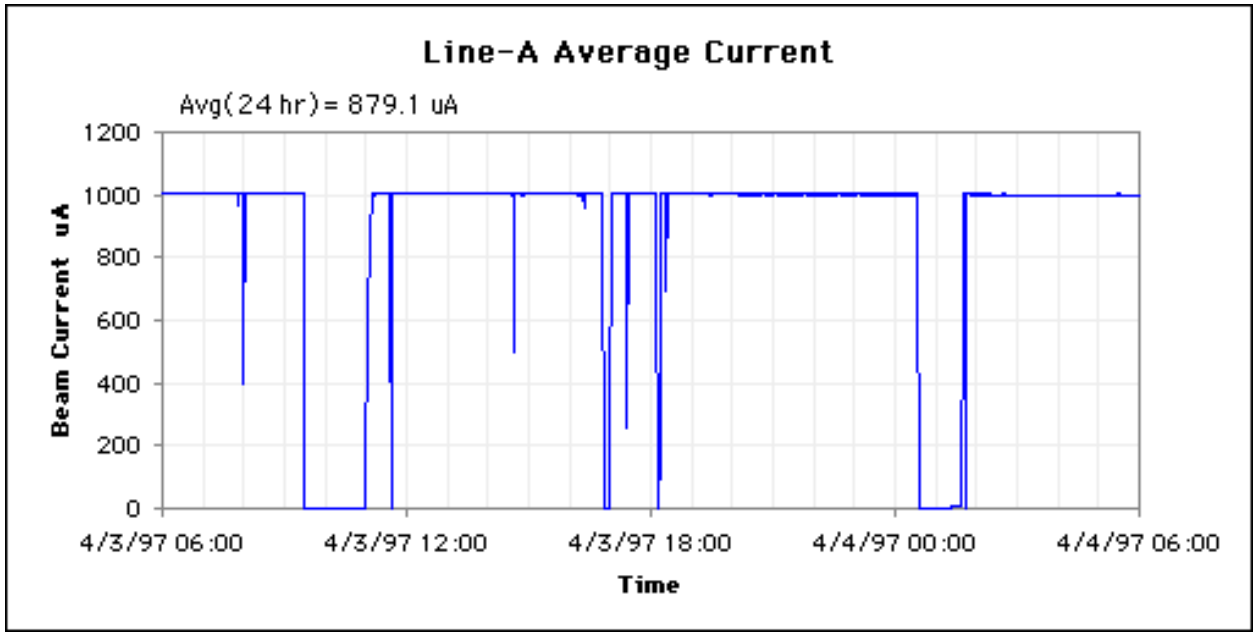

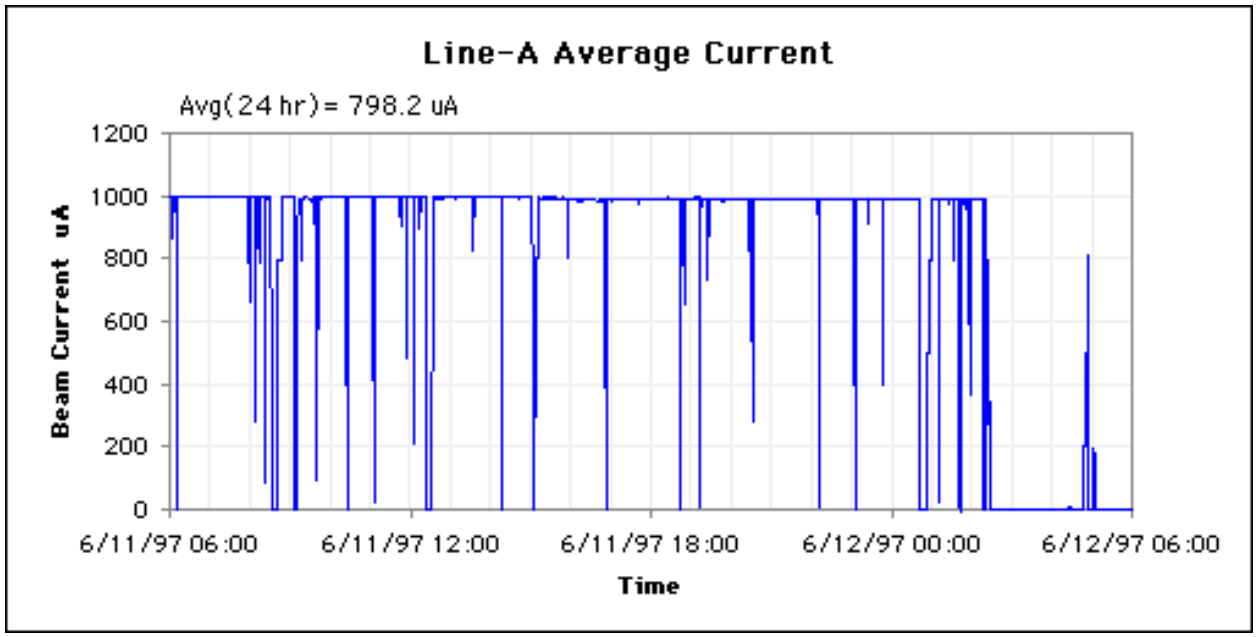

Figure 18 Beam current to the LANSCE A6 Target Station for two 24 hr periods. During **a)-top** early irradiation times beam on/off cycles were less frequent as compared to **b)-bottom** later times in the irradiation cycle. The only data presented in this study were collected during periods where the beam current maintained a steady current over the course of the EIS measurement (approx. 1.75 hrs).

Mechanistic Considerations While the mechanism by which corrosion rates are increased in the presence of high energy proton irradiation is not entirely understood, it is clear that its effects are to some degree reversible. This is demonstrated in Figure 19. In these experiments EIS data were collected before irradiation, during irradiation at 40 μA, 3 hrs after irradiation at 40 μA, and immediately after irradiation at 40 μA (labeled "instant off" in Figure 19). In an attempt to collect as much "near dc" data as rapidly as possible, the instant off data were only collected between the frequencies of 0.10 and 0.01 Hz which resulted in a minimal 20 minute measurement time. The steady-state polarization resistance measured during irradiation at 40μA was approximately 8 $x10^3$ ohms. The polarization resistance before and after irradiation was the same and equal to approximately 4 $x10^4$ ohms. This observation that the polarization resistance returns to its pre-irradiation levels after the beam is turned off is evidence that the damage which is caused proton irradiation is reversed at some time after irradiation. It may also be noted that the slopes of the 40 μA

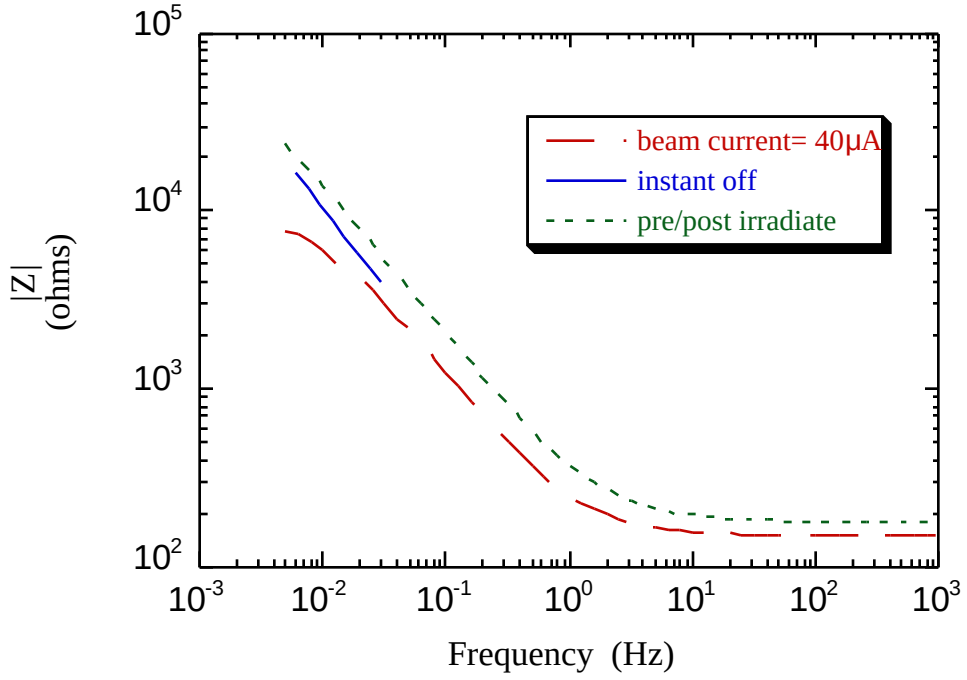

Figure 19 Bode magnitude data for the in-beam IN718 probe (corrosion insert only) showing gradual decay of the impedance to it's original pre-beam value after irradiation at 40 μA.

data and pre/post irradiation data between 0.03 and 1.0 Hz are equal to -1, as anticipated for capacitive behavior. For the instant off measurement, |Z| the magnitude of the impedance (|Z|) is greater than the |Z| during irradiation but less than the pre/post irradiation value. Moreover, the instant off data as a slope greater than -1. This behavior is indicative of a changing system, that is, the instant off data was non-steady state and the probe's response became more post-irradiation-like (and consequently less in-beam like) with increasing time after the beam was turned off.

While the mechanism by which proton irradiation increases the corrosion rate of IN718 is not yet understood, the possible effects of long-lived radiolysis products, short lived radiolysis products and direct proton / sample interactions are presented in terms of the results of this investigation. *Mechanism 1*: long-lived water radiolysis products. Long-lived radiolysis products are defined here as those species that are thermodynamically stable in the water system under operating temperatures and, as a result, their concentration in the system may build up over days, weeks, or months. They include products such as hydrogen, oxygen (O_2) and hydrogen peroxide (H_2O). As will be discussed in later publications, the peroxide concentration in this water system was measured after 4 months of irradiation and found to be approximately 0.34×10^{-3} M. Long-lived radiolysis products such as O_2 or H_2O are cathodic reactants and, therefore, will increase cathodically limited corrosion rates. Experimentally, one would expect to observe an increase in the open circuit potential (OCP) of the material if an increase in the concentration of cathodic reactants has occurred. This was observed during the LANSCE experiments as seen in Figure 20. However, an increase in OCP alone does not prove that an increase in the concentration of cathodic reactants is the cause of the observed increase in corrosion rates. As will be presented in later publications, no increase in OCP was observed in any of the out-of-beam probes when the beam was turned on. Although these cathodic reactants are being continually produced, it is clear from this result that their concentration was not sufficient at early irradiation times to effect the electrochemistry of the in-beam or out-of-beam samples.

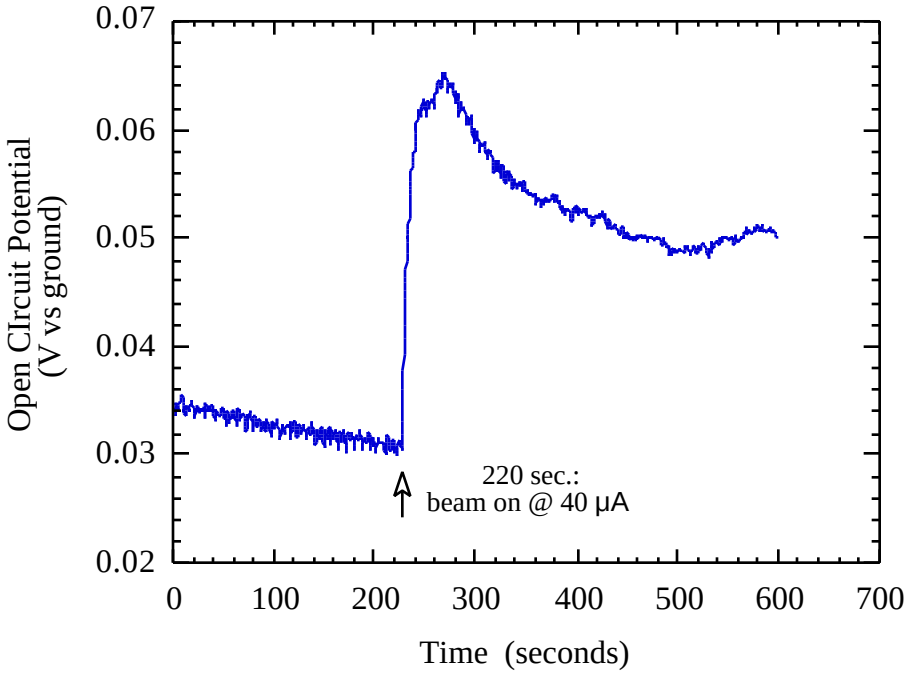

Figure 20 Open circuit potential as a function of time for the in-beam IN718 probe prior to and during irradiation at 40 μA. Because no reference electrode capable of withstanding irradiation by an 800 MeV proton beam exists, the OCP was measured with respect to the SS304 water system (ground).

Mechanism 2: short lived radiolysis products. Short-lived water radiolysis products are defined here as those species which are not thermodynamically stable in this water system, such as OH, $e^-_{aq,}$ HO_2, and O_2^- to name a few. These species do not build up in the system over the course of days or weeks as they typically have a life-time of less than $1x10^{-3}$ sec before recombining with other radiolysis products. For this reason any effect they may have on corrosion rate would be anticipated to only occur at the proton beam / water / IN718 interface as they are continuously formed and annihilated at this point. As may be anticipated, short lived species should not effect the OCP or corrosion rate of out-of-beam samples. However, the slow decay (> 20 min.) of the in-beam IN718 polarization resistance back to its pre-beam value as seen in Figure 19 would tend to rule this mechanism out.

Mechanism 3: direct proton / sample interactions. Radiation effects in materials comprise a wide range of phenomena. Physical damage in the material (which occurs ballistically below 1-10 MeV irradiation) may take the form of amorphitization or an increase in vacancy and dislocation concentrations. Radiolytic transfer of kinetic energy may also cause this type of damage. If, however, the energy of the ionizing radiation is sufficiently high, it may impart enough energy to valence electrons such that they are promoted to the conduction band. Although many of the electron-hole pairs that form in this manner recombine instantly (geminant recombination), those which escape this phenomena are free to migrate in an electric field. This is known as radiation induced conductivity (RIC) and accounts for the relatively high conductivities observed in otherwise insulating materials during high energy (>10 MeV) irradiation. The LANSCE A6 target station provides a unique combination of both high energy particles (800 MeV protons from the accelerator) and low energy spallation products (for example, neutrons). These spallation products result from direct proton interactions with the IN718 sample and other high Z number samples in the 17A and 18A-C inserts (such as W). Currently we are investigating the effects of high energy proton irradiation on the properties of passive oxides (with Surface Enhanced Raman Spectroscopy) and the electrochemical behavior of materials at the Weapons Neutron Research Facility.

System Calibration

The equipment used to make the IN718 in-beam corrosion rate measurements was calibrated by the manufacturer prior to shipment in 1996. In preparation for the FY '98 irradiation, this equipment was sent back to the manufacturer for calibration in November of 1997. As of December 1, 1997 these systems have been calibrated to NIST traceable registry numbers: 10071, 10072, and 10073. Current records of system calibration are available upon request.

To insure that the experimental equipment had functioned properly and the data obtained from the irradiation were reliable, a system test was employed. In this test, data was obtained from an electrical circuit containing a combination of parallel resistors and capacitors. The electrical

circuit used in these tests simulated an electrochemical response of an electrode in solution (Figure 21). The values used for the components were varied, and chosen to cover the range of values measured during the FY '97 irradiation. Representative Bode magnitude and phase data from the test circuit are shown in Figure 22. Also shown in this figure are the results from a complex non-linear least squares (CNLS) fit to the data. Excellent agreement between the experimental data and the curve fit were observed. A summary of the parameters from CNLS fitting of the data is presented in Table 1. The experimental data in Table 1 is in good agreement with the values of the resistors and capacitors quoted by the manufacturer. As these tests were performed after the '97 irradiation, we conclude that the experimental equipment was functioning properly and the data obtained from the irradiation were reliable.

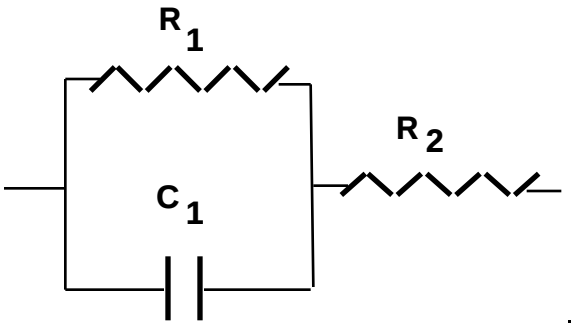

Figure 21 Diagram of the circuit used to verify the calibration of the EIS systems used to make the in-beam measurements presented in this study.

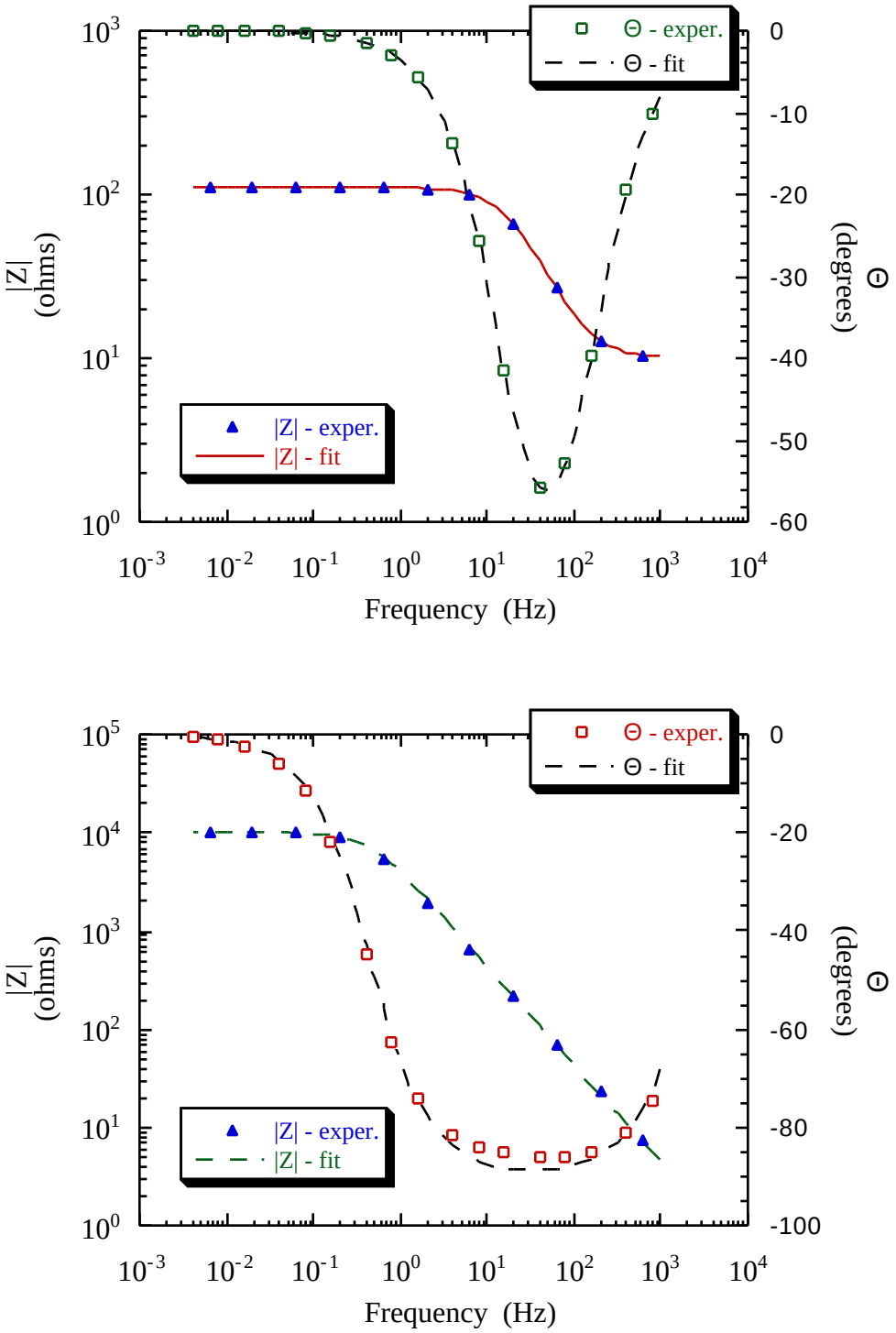

Figure 22 Typical Bode magnitude and phase data from the test circuit of resistors and capacitors (Figure 21) for **a)** R_1=100 Ω, C_1=1x10^{-4} F, R_2=10 Ω and **b)** R_1=1x10^4 Ω, C_1= 3.3x10^{-5} F, R_2=1 Ω.

Table 1 System verification results for all three systems used during the A6 irradiation period. Data was obtained from CNLS fitting of EIS data measured for the test circuit shown in Figure 21.

factory specified values (+/- 10%)		**values measured with system 02**	**values measured with system 08**	**values measured with system 10**
1)	R_1=100Ω	100Ω	100Ω	100Ω
	C_1=1x10^{-4}F	1.1x10^{-4}F	1.1x10^{-4}F	1.1x10^{-4}F
	R_2=10Ω	10.2Ω	10.4Ω	10.2Ω
2)	R_1=1x10^{4}Ω	9945Ω	9936Ω	9934Ω
	C_1= 3.3x10^{-5}F	3.68x10^{-5}F	3.69x10^{-5}F	3.69x10^{-5}F
	R_2=1Ω	1.74Ω	1.70Ω	1.72Ω

Summary

This report has described a method for measuring the real-time corrosion rate of materials during irradiation in an 800 MeV proton beam at the LANSCE A6 Target Station. EIS measurements have demonstrated that the polarization resistance of IN718 decreases from approximately 3x10^5 ohms prior to irradiation to approximately 1000 ohms during irradiation at a proton beam current of 400 μA. From the polarization resistance measurements, corrosion rate as a function of beam current was calculated for several different scenarios of beam / sample interaction. As the beam spot was small relative to the size of our IN718 corrosion probe (2σ=3 cm vs. 1.3 cm diam. x 15.9 cm length respectively), the first method for calculating corrosion rate used beam profile as a criterion for the area of highest damage. The beam spot intensity profile at LANSCE has been characterized and found to be a Gaussian distribution rotated about a central axis. From this relationship, and R_p as a function of beam current, corrosion rate as a function of radial distance from the center of the beam was calculated for each beam current. Physical evidence from change in thickness measurements made on tungsten rods irradiated at 1 mA during the FY 96 irradiation period suggest that this Gaussian damage profile is an accurate depiction of beam / sample interaction. From this method the corrosion rate of IN718 during irradiation at a

beam current of 1.0 mA is calculated to be approximately 0.002" per yr (2 mpy). The second method assumed that the predominant contributor to the corrosion current comes from an area defined by 2σ. Further, the method assumed that the corrosion rate was uniform over this area. Specifically, the R_p was multiplied by the area $\pi d \times 2\sigma$ where d was the diameter of the probe and equal to 1.3 cm. From this method the corrosion rate of IN718 during irradiation at a beam current of 1.0 mA is calculated to be approximately 0.001" per yr (1 mpy). The third method to calculate corrosion rate assumed that the distribution of corrosion was uniform across the entire surface. To calculate CR, the measured polarization resistance (R_p) was multiplied by the total probe area (approximately 63.3 cm^2). From this method the corrosion rate of IN718 during irradiation at a beam current of 1.0 mA is calculated to be approximately 0.0002" per yr (0.2 mpy). However, this rate is non-conservative and may be viewed only as a minimum corrosion rate.

The implication of the measured corrosion rate as a function of beam current as it applies to Accelerator Production of Tritium project is not yet clear. For example, the proposed APT beam will be rastered. This may have the same effect as the 100 Hz repetition rate of the beam at LANSCE, however this is still being analyzed. In addition, the APT proton beam will be operating at an energy of 1.7 GeV and a current of 1 mA. This differs from the beam at the LANSCE A6 Target Station. Currently, we are exploring a method for relating the in-beam corrosion rates measured at the LANSCE A6 Target Station to the APT beam profile, energy, flux, and current.